Journal of Power Sources 194 (2009) 899–907

Contents lists available at ScienceDirect

Journal of Power Sources

journal homepage: www.elsevier.com/locate/jpowsour

Spatially resolved degradation effects in membrane-electrode-assemblies of vehicle aged polymer electrolyte membrane fuel cell stacks

F. Ettingshausen [a,*], J. Kleemann [b], M. Michel [a], M. Quintus [b], H. Fuess [a], C. Roth [a]

[a] Renewable Energies, Institute for Materials Science, Technische Universität Darmstadt, Petersenstr. 23, D-64287 Darmstadt, Germany
[b] Fuel Cell System Development, Daimler AG, Wilhelm-Runge-Str. 11, D-89081 Ulm, Germany

ARTICLE INFO

Article history:
Received 18 March 2009
Received in revised form 28 May 2009
Accepted 2 June 2009
Available online 11 June 2009

Keywords:
TEM
Fuel cells
Degradation
Spatially resolved
Precipitates
Cell resistance

ABSTRACT

State of the art MEAs were aged in a fuel cell vehicle and degradation effects analyzed using electron microscopy and electrochemical methods. All cells of the stack showed a performance decay along with a loss in the electrochemical surface area. This could be correlated to particle growth and carbon corrosion observed by electron microscopy. Spatially resolved investigations showed a significant deterioration of the cathode, which is particularly pronounced at the hydrogen inlet. Differences in the cell performance of the aged cells could not be attributed to a variation in the catalyst degradation, but are linked to an altered ohmic resistance in the cells. The ohmic resistance of the cells is likely to be affected by the formation of precipitates in the membrane and seems to be correlated with their size.

1. Introduction

Polymer electrolyte membrane (PEM) fuel cells are a promising candidate for low to zero emission solutions in fuel cell vehicles. One of the crucial factors hindering a commercial market launch of this technology is the limited durability of the membrane electrode assembly (MEA). Both the deterioration of the carbon support and the catalytic nanoparticles in the catalyst layer strongly affect the performance and therefore the lifetime of the MEA. The presence of Pt catalyzes the oxidation of carbon and therefore its corrosion [1] while a deterioration of the carbon support accelerates the agglomeration of the Pt nanoparticles [2]. Preliminary studies [3] give witness of a strong link between fuel cell durability and working conditions of the cell.

Thermodynamically, the oxidation of carbon starts to occur at potentials above 207 mV versus normal hydrogen electrode (NHE) [4]. However, high corrosion rates only appear at much higher potentials above 800 mV [1]. To improve the durability of the electrodes graphitized carbon supports, which are more stable against corrosion [5], can be used. Platinum dissolution appears at relatively high potentials above 900 mV [6]. However, corrosion phenomena observed for constant potentials are less crucial compared to corrosion under dynamic conditions [7–9]. Furthermore, fuel cells used in a vehicle suffer from additional decay mechanisms like an up to 1.5 V increased cathode potential during the start up of the cell [10,11], caused by a hydrogen/oxygen front crossing the anode during the start up process. Another corrosive condition appearing at the anode is due to the hydrogen starvation at the anode, which can result in extremely high and thus corrosive potentials [12,13]. Consequently, precise durability investigations of fuel cells for automobile applications have to closely mimic a real life load profile, in order to account for the degradation effects that are depending on the working conditions.

Transmission electron microscopy (TEM) is a suitable method to follow MEA degradation. In several studies the formation of Pt precipitations in the polymer membrane has been observed [14–17]. Yasuda et al. [14] assume this formation of platinum crystallites in the membrane to be due to platinum dissolution at the cathode and successive platinum migration and deposition in the polymer electrolyte membrane. High potentials at the cathode dissolve part of the platinum nanoparticles into an ionic platinum species, which can migrate into the membrane. Crossover hydrogen from the anode reduces the platinum ions in the membrane, leading to the formation of crystallites. On the contrary, crossover oxygen can suppress the formation of precipitates in the membrane. Hence, the site where the precipitation band can be observed moves toward the anode when the hydrogen concentration decreases or the oxygen concentration increases in the membrane. The reduction processes of migrated platinum ions and the re-oxidation of

* Corresponding author. Tel.: +49 6151 16 5498; fax: +49 6151 16 6023.
E-mail address: ettingshausen@st.tu-darmstadt.de (F. Ettingshausen).

0378-7753/$ – see front matter © 2009 Elsevier B.V. All rights reserved.
doi:10.1016/j.jpowsour.2009.06.003

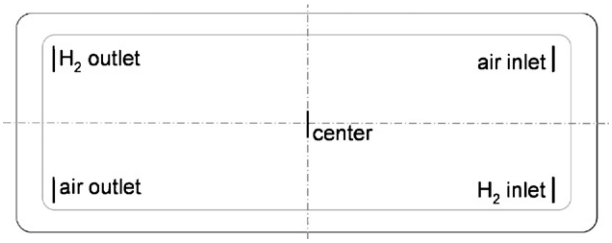

Fig. 1. Schematic drawing of the regions of the MEA, which have been investigated by TEM.

the precipitations can be described as follows [15]:

$$Pt^{2+} + H_2 \rightarrow Pt + 2H^+$$

$$Pt + 1/2O_2 \rightarrow PtO$$

$$Pt + O_2 \rightarrow PtO_2$$

$$PtO + 2H^+ \rightarrow Pt^{2+} + H_2O$$

The concentration of the crossover hydrogen and oxygen does not only determine the local position of the precipitation band [14], but it also strongly affects the distribution and the particle size of the re-precipitated platinum crystallites. While higher concentrations of hydrogen and oxygen cause well defined and narrow precipitation bands with big crystallites, lower concentrations result in a broader region of deposited Pt with a comparatively smaller particle size [15]. Under certain conditions, e.g. low crossover hydrogen, platinum ions from the cathode can migrate through the whole membrane all the way up to the anode side [15], where the re-precipitation of these ions takes place more easily on the surface of the platinum nanoparticles than on the carbon support [16]. This leads to the observation of higher metal loadings at the interface between anode and membrane.

The MEAs with carbon-supported catalyst that have been investigated in this report have undergone real world testing in a fuel cell vehicle. In this prototype vehicle a special focus was put on start-up and shut-down behavior of the fuel cell stack, so that an artificially high number of starts had occurred during the operational time of the stack. Besides a general performance degradation in all cells after some hundred hours of operation, some cells showed a severe higher-than-average performance loss that even led to infrequent cell breakdown events in those cells. After disassembly of the degraded stack some of the cells with unexpected high performance decay as well as some cells with normal performance decay were tested in single cell setups. Furthermore, also some new MEAs of the same type were tested in the same single cell setup for reference. This procedure aimed at a more precise characterization of the degradation effects especially in those critical cells.

Up to now a lot of research has focused on the degradation of the MEAs over the entire area. However, spatially resolved degradation studies are scarce. For the MEAs investigated in this study, TEM analysis of different regions of the MEA (anode inlet/outlet, cathode inlet/outlet and center) was carried out at ultra-thin cross-sections. Fig. 1 schematically shows the regions of the MEA, which have been investigated by TEM.

2. Experimental

Commercial MEAs comprising carbon-supported platinum catalysts have been aged in a stack by real world testing in a prototype fuel cell vehicle as described above. The MEAs had an initial platinum loading of 0.4 mg cm^{-2} on both anode and cathode and the platinum was supported on a non-graphitized carbon. To check the performance of the MEAs used in the stack after aging, polarization curves were recorded under undersaturated constant pressure conditions. In these polarization tests, relative humidity of the feed gases was set to 40% on both anode and cathode at a cell temperature of 85 °C. Gas utilization was 60% for hydrogen and air at all load points down to 0.1 A cm^{-2}, whereas for further decreased current densities flow rates were kept constant relative to 0.1 A cm^{-2}. For selected samples in situ cyclic voltammograms (CV) were measured to allow for a characterization of remaining active platinum surface area and hydrogen crossover. The cyclic voltammograms were recorded by flushing the cell with saturated nitrogen on the testing electrode and saturated hydrogen on the reference electrode. Five potential cycles between 0.06 and 1.2 V were conducted at 20 mV s^{-1}. Only the last cycle was used for analysis and the measured current was corrected for hydrogen crossover and double layer capacity. The active platinum area was finally calculated from the hydrogen desorption area integral.

For selected samples different MEA regions (anode inlet/outlet, cathode inlet/outlet and center) of both the anode and the cathode were prepared for TEM analysis using ultramicrotomy. The cross-sections were compared to each other and to an unused MEA as a reference. TEM investigations have been performed using a Jeol JEM-3010 transmission electron microscope operating at 300 kV acceleration voltage with a LaB_6 cathode. Sample preparation for the TEM followed the procedure described by Blom et al. [18]. A piece of the MEA was removed and embedded in Araldite 502 resin (SPI Supplies, Inc.). The embedded sample was cured for 16 h at 60 °C. Afterwards, thin sections of the sample were prepared using a Reichert-Jung ultracut microtome at room temperature. These 70–100 nm thick sections were placed onto copper grids, where they were left to dry at room temperature for at least 48 h.

The cross-sections have also been investigated by a Zeiss 962 Scanning Electron Microscope. For the SEM measurements a specially designed sample holder, which supports the copper grids only on their outer rim, was used with the aim to minimize the interactions of the sample holder and the electron beam.

Since the Jeol JEM-3010 is optimized for high resolution pictures, only sample tilts between ±20° can be obtained. Hence, a Philips CM12 transmission electron microscope operating at 120 kV with a LaB_6 cathode was used to record selected area diffraction patterns using a double tilt holder. The Philips CM12 is equipped with an EDAX Genesis spectroscopy unit to record energy dispersive X-ray spectra (EDX). EDX spectra were recorded in the same experimental conditions, in which the diffraction patterns have been obtained. Diffraction pattern have been indexed by using the program PIEP [19].

Structural analysis of the TEM and SEM pictures was carried out to estimate the particle size of the platinum nanoparticles, the electrode thickness for the investigated MEA regions and the distance between the cathode and the precipitation band in the membrane, which was observed for the tested MEAs. To calculate a mean particle size of the platinum nanoparticles the diameter of about 170 particles was measured. The electrode thickness was determined from the SEM pictures of the ultra-thin cuts. Therefore, the electrode thickness of the anode and the cathode has been measured at three different places of the ultra-thin cut and the mean value was computed. To determine the distance between the precipitation band and the cathode the range between the interface membrane/cathode and one of the largest visible precipitations in the TEM picture was measured. Overall, this distance has been measured four times and afterwards a mean distance was calculated. The mean maximum precipitation size has been determined by calculating the mean diameter of the five largest precipitations that have been visible in the picture which was used for the investigation.

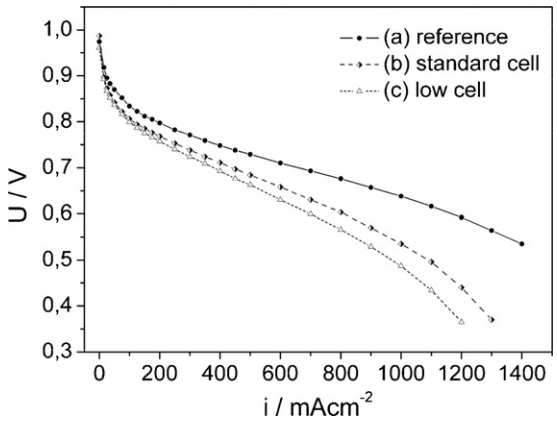

Fig. 2. Polarization curves of (a) the reference MEA, (b) the "standard cell" and (c) the "low cell"; the higher performance loss of the "low cell" compared to the standard cell appears in the ohmic region indicating a higher resistance.

3. Results and discussion

Fig. 2 shows the polarization curves which were measured in order to check the performance of the stack MEAs after ageing in conditions that mimic their real utilization. It appears that similar performances after ageing can be observed for the majority of the investigated MEAs. These samples will be called "Standard cells". Nevertheless, a small batch of the stack MEAs showed a higher performance loss, which might be attributed to a higher ohmic loss occurring in these membranes after ageing. These samples will be identified as "low cells" in the text. The additional performance loss of the "low cell" seems to increase linearly at a current density between 50 and 800 mA cm^{-2} in the so-called ohmic region of the polarization curve. Since the slope in the ohmic region does correspond to the electric resistance of the whole cells, the higher performance decay of the "low cells" might be due to a higher ohmic resistance. In the kinetic region, below a current density of 50 mA cm^{-2}, no significant differences can be observed for all tested aged MEAs, suggesting the same catalytic activity for all of them. As expected, the fresh MEA, used as a reference, presents the best performance, the highest catalytic activity and the lowest resistance.

Table 1
Electrochemical active surface area determined by CV measurements.

Sample name	Sample description	ECA anode ($m^2\ g^{-1}\ Pt^{-1}$)	ECA cathode ($m^2\ g^{-1}\ Pt^{-1}$)
Reference	Non-aged MEA	63.3	62.8
Standard cell	MEA exhibit "normal" performance decay	37.3	21.8
Low cell	MEA exhibit "high" performance decay	36.0	19.3

In order to better understanding this behavior additional cyclic voltammetry measurements (Fig. 3) and TEM studies were performed on a "low cell", a "standard cell" and on a non-aged reference MEA.

At a potential of less than 450 mV against NHE one can see the adsorption of hydrogen on the platinum surface at decreasing potential and the hydrogen desorption at rising potential [20]. OH adsorption can be seen at potentials higher than 550 mV and at even higher potentials (>800 mV) an oxygen layer is formed on the Pt surface. The active platinum surface area was calculated from the hydrogen desorption current corrected for hydrogen cross-over and double-layer capacity, assuming a covering layer capacity of 210 μC cm^{-2} Pt [20].

The electrochemical active surface area of the electrodes for the different MEAs determined by cyclic voltammetry is listed in Table 1. By comparing the two tested MEAs with the non-aged reference it is obvious that both aged samples have lost almost the same percentage of active surface area. About 60% of the initial reference

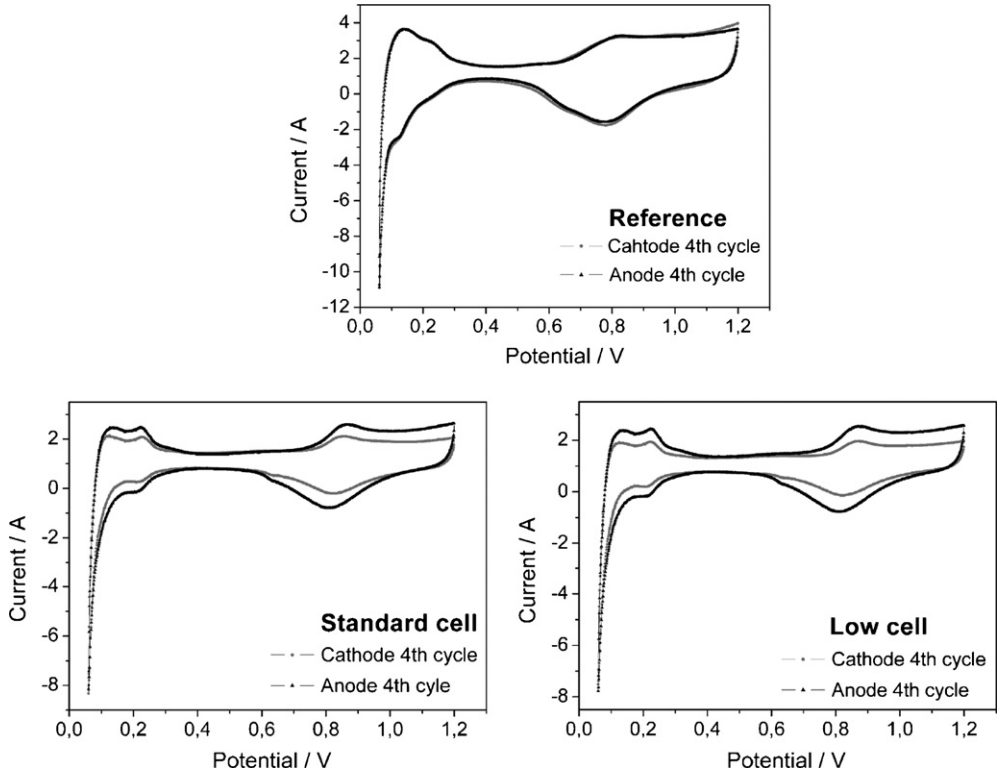

Fig. 3. Cyclo-voltammograms of the reference MEA, the "standard cell" and the "low cell".

Table 2
Resistance and catalytic parameters fitted to the polarization behavior of the different MEAs at oxygen partial pressure of 25 kPa.

Sample name	Polar. resistance (fit) (mΩ cm^2)	Specific activity (fit) @ 900 mV (mA cm^{-2} Pt)	Mass activity (fit) @ 900 mV (mA mg^{-1} Pt)
Reference	97	0.115	72
Standard cell	132	0.201	43
Low cell	171	0.205	39

area is left at the anode and about 35% Pt is left at the cathode. Thus, the difference in the polarization curves of the degraded samples cannot be explained by the results of the CV. A significant difference in total platinum area loss could not be found for those MEAs, as has already been presumed from the comparable kinetic behavior of the cells in the polarization experiments.

To provide a more quantitative insight into the behavior of the cells, an analytical interpretation of the measured polarization curves was conducted. It was assumed that three major terms dominate the voltage drop over current density, as is indicated by Eq. (1):

$$U_{\text{cell}} = U_0 - b \log i - iR_{\text{cell}} \quad (1)$$

A linear contribution of voltage drop over current density according to ohmic resistance R_{cell} and a logarithmic contribution b according to the Tafel slope as well as an open circuit voltage U_0 were fitted to the measured polarization curves using the least square method in the low current density region. Although the measured curves and conditions are not perfectly adequate for this type of interpretation, the results may well give a rough impression of the relative differences between the cells. The dry polarization conditions led to a drastic resistance increase at low current densities that might adulterate the results, because a constant resistance is assumed for the fit. Furthermore, a mass transport effect might be of some impact even in the low current density regime for these air polarization measurements [21]. However, only polarization measurements under these conditions were available initially and the MEAs were destroyed for post-mortem analysis. Nonetheless, fitted ohmic resistances and specific catalyst activities calculated from the fit at 900 mV as given in Table 2 seem to give a good first indication.

It becomes obvious that the fitted polarization resistance is significantly different between the cells and is rising from reference to "standard cell" and is again approximately 40 mΩ cm^2 higher for the low cell. Catalytic activity does not differ too much between the aged cells, but shows a distinct difference when compared to the non-degraded reference. Mass related activity representing current density at 900 mV (*iR*-corrected) per mg platinum initially used decreases by about 45% for the aged samples, mainly due to the decrease in active platinum area that was also found in the CV measurements. However, active platinum area on the cathode was found to be about 65% lower compared to the reference for the aged samples which is clearly more than the decrease in mass specific activity. This can only be explained by a gain in specific catalyst activity per catalyst surface area for the degraded samples that partly compensates the surface area loss. For larger platinum particles, a higher specific ORR activity can be expected following [21]. Larger particles were also found in this study for the degraded samples, as becomes obvious from the surface area loss but as will also be proven by the TEM results given below. According to those, the mean platinum particle size on the cathode has increased from 1.7 nm for the reference to more than 4 nm for the degraded MEAs. The gain in specific activity for the degraded catalysts can thus only be explained as an effect of the platinum particle growth during aging due to dissolution, migration and Ostwald ripening, that partially compensates the active area loss by higher Pt surface ORR activity.

However, no explanation for the increase in the ohmic resistance of the cells can be given, in particular it is not clear why the polarization resistance is significantly different for cells degraded in the same stack.

Therefore, additional TEM investigations were carried out in order to compare the micro-structure of the different cells. Cross-sections at significant regions of the MEA (anode inlet/outlet, cathode inlet/outlet and center) were investigated and compared in between one cell and between the both tested cells. However, by comparing the electrode micro-structure of those two aged cells against each other no significant differences were visible. Both cells were actually showing the same differences in the decay of the electrode for the investigated regions of the MEA cross-sections. Table 3 lists the average particle size and standard variation determined for the investigated regions.

3.1. Degradation effects in the electrode

The electrode degradation has been analyzed focusing on particle growth, change in dispersion and in electrode thickness. In general, more particle growth appears for the cathode compared to the anode, as can be seen in Table 3. However, this effect was expected due to the well known fact, that electrode degradation is more crucial at the cathode side. TEM images of the cathode structure are shown in Fig. 4 for the low cell and the reference MEA. At both the air inlet and the center of the MEA particle growth can be seen, but there is no significant agglomeration of the nanoparticles visible and no dominant corrosion effects of the

Table 3
Mean TEM particle size of the different investigated parts of the MEAs.

Sample name	Cathode		Anode	
	Mean particle size (nm)	Standard deviation (nm)	Mean particle size (nm)	Standard deviation (nm)
Reference	1.7	0.49	1.8	0.47
Standard cell H_2 inlet	4.2	1.15	3.3	1.06
Standard cell H_2 outlet	4.4	1.02	3.9	0.85
Standard cell air inlet	4.1	1.26	3.1	1.14
Standard cell air outlet	3.5	1.07	3.2	0.87
Standard cell center	4.5	1.37	3.9	1.22
Low cell H_2 inlet	5.2	1.84	3.4	1.17
Low cell H_2 outlet	4.7	1.28	2.9	0.89
Low cell air inlet	3.5	1.31	3.4	0.94
Low cell air outlet	4.4	1.19	4.0	1.10
Low cell center	4.0	1.73	3.4	1.20

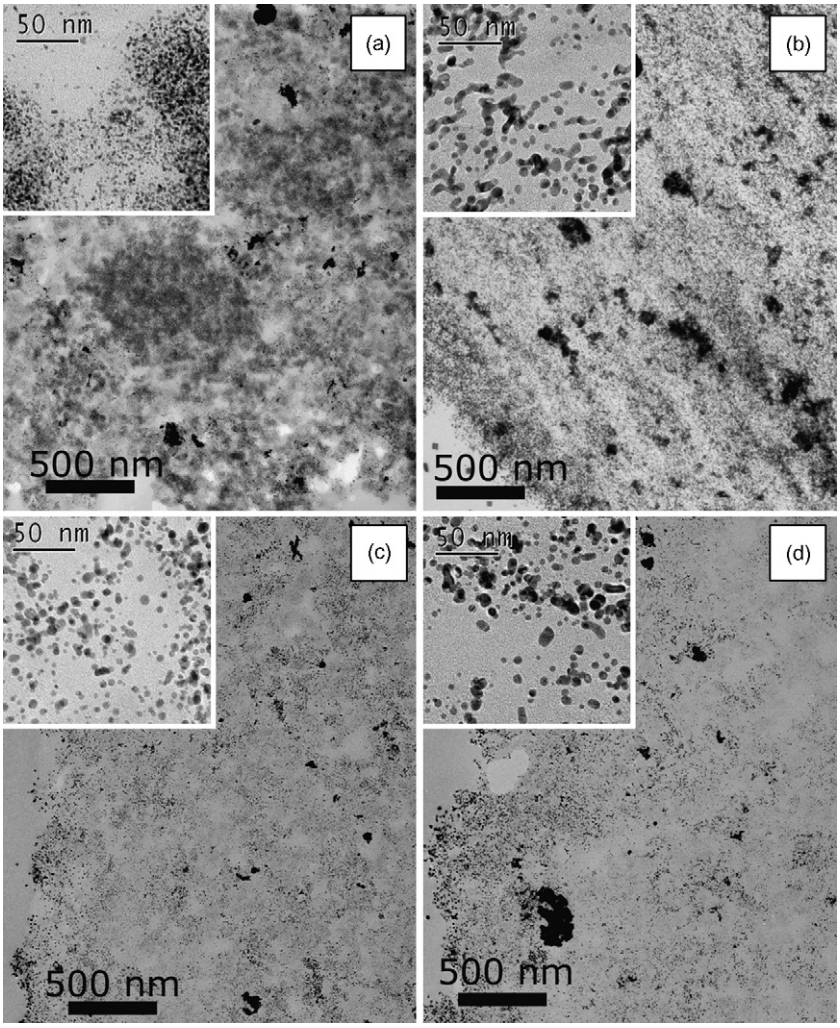

Fig. 4. Survey TEM pictures of the cathode: (a) reference, well dispersed Pt-particles (dark gray) on carbon support (light gray) are visible; (b) low cell at hydrogen inlet, almost no carbon support could be observed, strong agglomeration of the Pt-particles can be seen; (c) low cell at air inlet, still good dispersion of the catalyst, particle growth; (d) low cell at center, particle growth and homogeneously dispersed catalyst particles.

carbon support were observed. However, in the region of the hydrogen inlet a strong deterioration of the cathode is visible for both degraded samples. Furthermore, by measuring the thickness of the electrodes from the cross-sections in the SEM, the most pronounced decrease of the electrode thickness can be determined for the region at the hydrogen inlet (Table 4). This decrease is proposed to be due to strong carbon corrosion. A significantly increased cathode potential during the start up process of the cell, which is caused by a hydrogen/oxygen front in the anode is reported in the literature [10]. Directly at the hydrogen inlet, the cathode potential should be highest due to a well defined hydrogen/oxygen front in this region. Going further towards the anode outlet, the developing gas front is expected to be less pronounced and therefore lower cathode potentials and less degradation should occur.

Table 4
Measured SEM electrode thickness of the different investigated parts of the MEAs.

Area	Anode (μm)			Cathode (μm)		
	Low cell	Standard cell	Reference	Low cell	Standard cell	Reference
Center	12.8	13.6	14.7	10.0	11.7	15.6
Air inlet	11.6	14.4		13.6	12.4	
Air outlet	11.2	9.8		11.8	10.2	
H_2 inlet	13.6	12.6		3.1	2.2	
H_2 outlet	12.2	8.2		9.1	4.3	

By observing the interface between the electrodes and the membrane a higher metal loading was detected directly at the interface membrane/electrode as shown in Fig. 5. This effect is much more pronounced at the interface anode/membrane and just slightly visible at the interface cathode/membrane. Preliminary studies [16] have shown that the deposition of dissolved platinum ions occurs likely on a platinum surface. We expect the increased metal loading at the interface anode/membrane due to platinum ions, that got dissolved at the cathode and afterwards have migrated across the membrane and finally deposited at the "first" platinum particles of the anode. Since at the cathode the platinum ions got dissolved due to high potentials under certain conditions, only few ions directly deposit at the platinum particles at the interface cathode/membrane if potential there becomes low enough for redeposition.

3.2. Degradation of the MEA

The formation of re-precipitated Pt crystallites in the membrane was found for both aged cells. Between anode and cathode a gradient in the particle size of these precipitations can be observed. Close to the interface of the cathode and the membrane, the formation of small crystallites appears. The crystallite size increases towards the

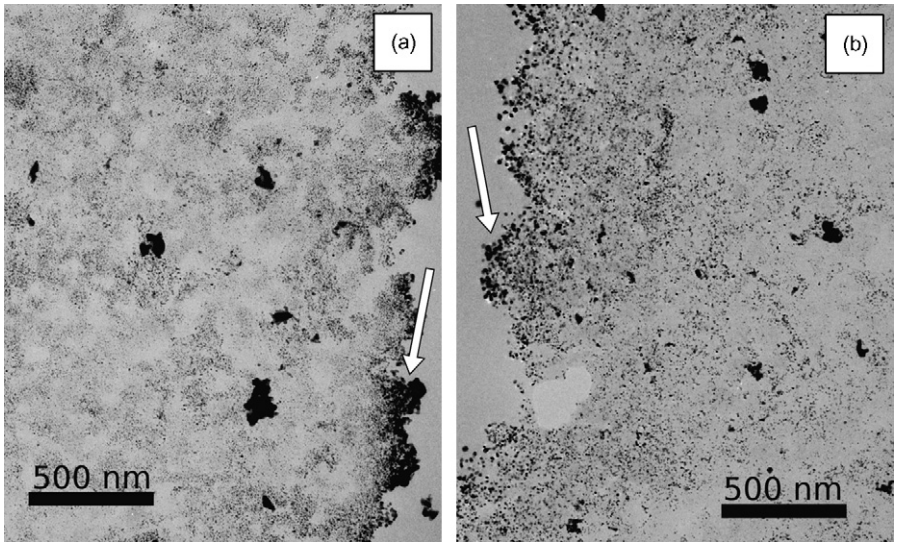

Fig. 5. TEM pictures of the center of the low cell; marked by an arrow an increased platinum loading is observed, which is significant for the interface anode/membrane (a) and less so for the interface cathode/membrane (b).

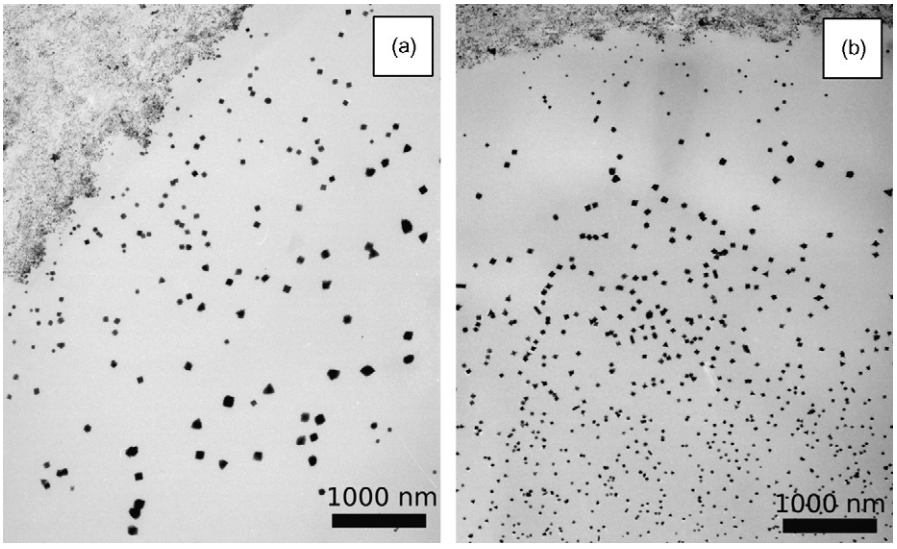

Fig. 6. TEM investigations of the interface between cathode and membrane in the region of the H_2 outlet (a) for the low cell comparatively larger re-precipitated platinum crystallites can be observed than (b) for the standard cell.

anode and after a distance of about 1–3 μm for the standard cell and 2–4.5 μm for the low cell reaches a band of precipitations with a maximum diameter (Fig. 6). The exact values are also dependent on the area where the measurements were taken. By going further to the anode, the precipitation size decreases again. It is observed that the formation of this precipitation band of crystallites with a maximum diameter depends on the hydrogen and oxygen crossover. The influence of the reactants and the reason for the formation of the precipitations has been discussed in studies by Yasuda et al. [14]. Platinum ions from the cathode migrate across the membrane and can get reduced from crossover hydrogen, leading to the formation of the observed precipitations in the membrane. Oxygen crossover from the cathode suppresses the formation of the re-precipitated platinum crystallites. Therefore, the amount, size and distribution of the precipitations in the membrane are strongly affected by the crossover hydrogen and crossover oxygen which corresponds to the hydrogen and oxygen partial pressure at the anode and the cathode.

In Table 5 the estimated distances between precipitation band and the cathode as well as the maximum precipitation diame-

Table 5
Maximum precipitation size observed in the membrane and estimated distance between cathode and precipitation band.

Sample name	Distance cathode and precipitation band (nm)	Max. precipitation size (nm)
Standard cell H_2 inlet	1230	118
Standard cell H_2 outlet	1590	67
Standard cell air inlet	2700	62
Standard cell air outlet[a]		
Standard cell center	2900	107
Low cell H_2 inlet	4560	196
Low cell H_2 outlet	2510	137
Low cell air inlet	3680	176
Low cell air outlet	3690	147
Low cell center[b]	3250	229

[a] Due to high amount of precipitations; the membranes of all thin cuts of this region were ripped and therefore no max. precipitation size and distance between cathode and precipitation band could be estimated.

[b] To calculate the mean distance between cathode and precipitation band as well as to determine the mean max. precipitation size only two values have been measured for both, distance and size.

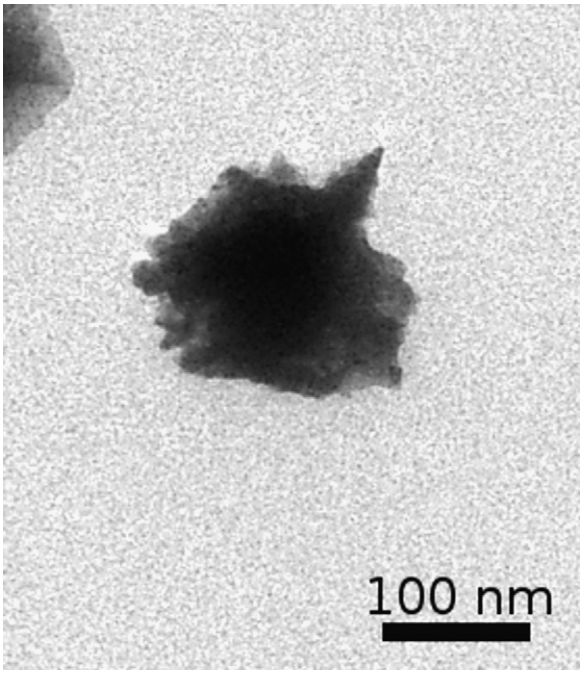

Fig. 7. Precipitation in the membrane with frayed edges as observed by TEM.

ters for the different investigated MEAs and regions are listed. Re-precipitated Pt crystallites can be observed over the whole width of the membrane. Furthermore, a well defined shape of those crystallites is visible. Cubic, tetragonal and triangular precipitations can be seen. Comparing the low cell and the standard cell, it is obvious that larger precipitations can be found for the low cell. While for the standard cell crystallites with a maximum particle size up to 120 nm are present, for the low cell crystallites with a maximum particle size up to 230 nm are visible. The differences in the size and distribution of the precipitations could be supposed to be the reason for the worse performance of the low cell.

It has been shown above that the difference in performance between aged standard and low cell can mainly be attributed to a higher cell resistance. The lowest resistance can be determined for the non-aged reference MEA, which of course does not contain any precipitations in the membrane. Therefore, we suggest the crystallites in the membrane decrease its proton conductivity. It is likely that precipitations will evolve in the proton conducting hydrophilic channels of the membrane in proximity to the sulfonic acid groups, which should also be a preferred allocation site for metallic ions. Precipitations of solid metal crystals growing in the ion channels block them for proton transport thereby increasing the resistance of the membrane. Besides the blockage phenomena obtained by the metallic precipitates, also platinum ions can block the sulfonic groups and may also lead to an increased resistance of the membrane.

By observing the shape of precipitations with a diameter of at least 100 nm, no more well defined shapes of the crystallites are visible. In Fig. 7, the frayed edges of a precipitated crystallite are shown. We assume this precipitation shape to be a result of crystallite growth into the ion channels of the membrane. If the size of the precipitations reaches a certain diameter, particle growth proceeds into crossing ion channels, resulting in a frayed shape of the crystallites. The size of the platinum crystallites seems to be critical in terms of ion channel blockage, since the low cell with larger crystallites had shown a significantly increased resistance in the polarization compared to the standard cell, even though the membrane in the standard cell showed a similar number of crystallites.

However, a difference in ohmic resistance between the cells could not be found in the high frequency resistance measurement during polarization measurements, that was consequently lower than the fitted resistance for all cells. The reason becomes clear when the structure of the crystallites is taken into account. Due to their metallic nature the precipitations act as an electron conductor, whereas on the other hand they act as a blockage for a directed protonic current as occurring during cell operation. For the high frequency current however, this barrier is passable since a metallic electrode–electrolyte boundary as an interface between electronic and ionic current is not affecting the high frequency current following [20].

Again differences are visible for the different investigated regions of the MEAs. The number of crystallites in the membrane near the anode varies significantly. At the anode in the region of the air outlet a high number of precipitations can be observed compared to the air inlet (Fig. 8). We assume those differences to be due to a change in H_2 and O_2 partial pressure occurring at the different areas of the MEA in good agreement with studies by Yasuda et al. [14]. For the air outlet a lower oxygen concentration compared to

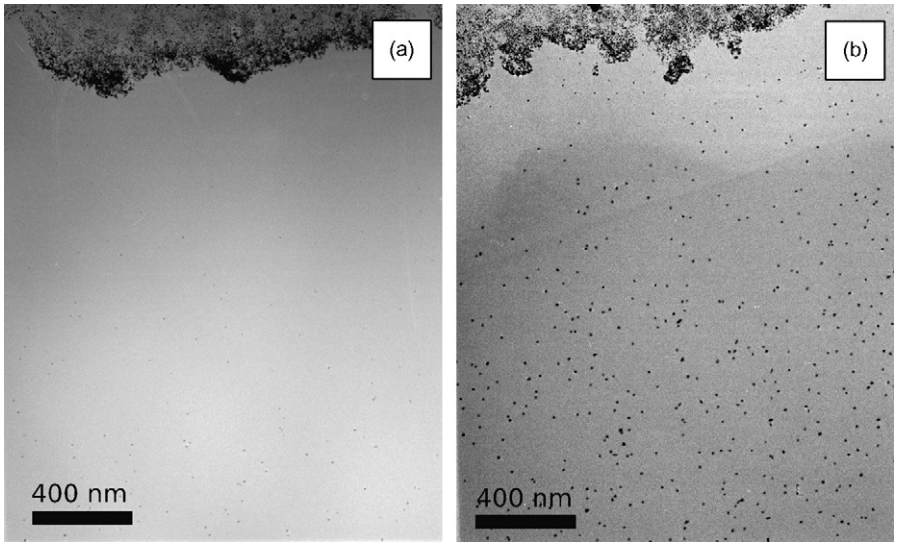

Fig. 8. TEM pictures of the low cell at the interface between anode and membrane: (a) membrane in the region of the air inlet and (b) membrane in the region of the air outlet.

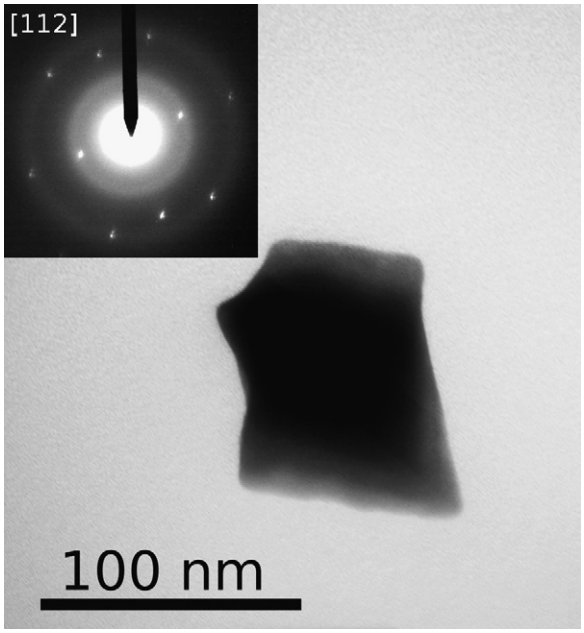

Fig. 9. TEM investigation of a precipitation in the membrane of the standard cell (MEA center), the SAD pattern on zone axis 1 1 2 belongs to the cubic platinum phase.

the air inlet is likely. While oxygen suppresses the formation of precipitations in the membrane, less precipitations can be found at the air inlet as compared to the air outlet.

To determine the chemical composition of the precipitations – representative for the rest of the observed precipitations – EDX spectra were recorded for the standard cell in the region of the MEA center. From the EDX spectra it is clear, that the crystallite precipitations contain platinum.

Since from the EDX spectra the composition of the precipitations cannot be clearly attributed to pure platinum, selected area electron diffraction (SAED) was performed at crystallites at the same areas, which have been investigated by EDX. The diffraction patterns should help to clarify if the precipitations are pure platinum crystallites or if they are composed of more than one phase containing also some other elements. For each crystallite at least three different diffraction patterns, related to different zone axes, have been recorded. All zone axes were indexed with the cubic structure of pure platinum. In Fig. 9 the diffraction pattern along the 1 1 2 zone axis is shown. The lattice distance which can be determined from the diffraction patterns, is about 3.7 Å, while the theoretical binding length for platinum is about 3.9 Å. However, binding lengths calculated from TEM diffractions are less precise than binding lengths measured by X-ray diffraction (XRD).

4. Conclusion

Different performance decays were observed for MEAs tested in the same stack under real world conditions. A majority of MEAs (standard) was showing almost the same performance loss with time, while a minority of MEAs (low) suffered from a comparatively higher performance loss. Since no difference in the electrochemically active surface area was visible for the standard and the low cell determined by cyclic voltammetry and since the catalytic activity also seemed comparable, detailed investigations of the MEA structure were carried out using TEM and SEM.

Comparing the electrode structure of the standard and low cell, no significant differences were visible. Both MEAs showed similar electrode structures, although the structure itself varied for the different regions investigated (anode inlet/outlet, cathode inlet/outlet and center). A very significant deterioration of the cathode appears in the region of the hydrogen inlet, possibly due to the harsh conditions during air–air start-up in this region. Plenty of precipitations were observed in the membrane of both analyzed MEAs. EDX spectra and SAED patterns clearly identify these precipitations to be pure platinum crystallites. Size and distribution of those precipitates also depend on the investigated regions of the MEA.

For the low cell comparatively large precipitations with a diameter up to 230 nm were visible, while for the standard cell only precipitations with a diameter up to 120 nm have been observed. It is expected that the platinum crystallites grow in the ion channels of the membrane and therefore decrease the proton conductivity of the membrane. In recent studies [22], Ohma et al. also observed accelerated membrane degradation nearby a band of Pt precipitations in the membrane. It is possible, that this enhanced membrane degradation due to the Pt precipitations also lowers the proton conductivity of the membrane. From the polarization curves of the MEAs it is found, that the higher performance loss of the low cell compared to the standard cell is due to a higher ohmic resistance of the low cell. Consequently, MEAs containing larger precipitations in the membrane also seem to show higher ohmic resistances.

In preliminary studies we were able to attribute the formation of Pt precipitations in the membrane to the harsh conditions during the start-up process of the cell due to a hydrogen/oxygen front which is crossing the anode. Since the position of the low cells in the stack does not show a distinct pattern, but appears more like a statistical distribution, a variation in the cells is likely to provoke locally enhanced degradation and thus larger precipitations in some cells during start-up. A possible source is the residence time of the hydrogen/air front in the particular cell that is mainly determined by flow distribution between the cells, a longer residence time causing higher degradation. An obvious reason for less flow share and thus for larger precipitations in the low cells could be a variation within the production tolerance of the flow fields. Due to this variation of the flow fields the hydrogen/oxygen front would cross slower through the anode of the low cells and therefore the low cells would be exposed to the harsh conditions for a longer time.

Acknowledgements

Financial support of the Federal Ministry of Education and Research (BMBF “KONNEKT”) has been gratefully acknowledged. The authors are grateful to G. Miehe and J. Kling for work on the SAED diffraction pattern and U. Kunz for her help in the preparation of the ultra-thin cross-sections.

References

[1] L.M. Roen, C.H. Paik, T.D. Jarvic, Electrochemical and Solid State Letters 7 (1) (2004) A19.
[2] Y.Y. Shao, G.P. Yin, Y.Z. Gao, P.F. Shi, Journal of the Electrochemical Society 153 (6) (2006) A1093.
[3] Y.Y. Shao, G.P. Yin, Y.Z. Gao, Journal of Power Sources 171 (2007) 558.
[4] K. Kinoshita, Carbon: Electrochemical and Physicochemical Properties, Wiley, New York, 1988, 319.
[5] D.A. Stevens, M.T. Hicks, G.M. Haugen, J.R. Dahn, Journal of the Electrochemical Society 152 (12) (2005) A2309.
[6] M. Pourbaix, Atlas of Electrochemical Equilibria in Aqueous Solutions, Pergamon, New York, 1966.
[7] K. Kinoshita, J.T. Lundquist, P. Stonehart, Journal of Electroanalytical Chemistry 48 (1973) 157.s.
[8] R.M. Darling, J.P. Meyers, Journal of the Electrochemical Society 150 (11) (2003) A1523.
[9] T. Patterson, Fuel Cell Technology Topical Conference Proceedings 2002 AIChE Spring National Meeting, March 10–14, 2002.
[10] C.A. Reiser, L. Bregoli, T.W. Patterson, J.S. Yi, J.D.L. Yang, M.L. Perry, T.D. Jarvi, Electrochemical and Solid State Letters 8 (6) (2005) A273.
[11] W.R. Baumgartner, P. Parz, S.D. Fraser, E. Wallnofer, V. Hacker, Journal of Power Sources 182 (2) (2008) 413.

[12] A. Taniguchi, T. Akita, K. Yasuda, Y. Miyazaki, Journal of Power Sources 130 (1–2) (2004) 42.
[13] S.D. Knights, K.M. Colbow, J. St-Pierre, D.P. Wilkinson, Journal of Power Sources 127 (1–2) (2004) 127.
[14] K. Yasuda, A. Taniguchi, T. Akita, T. Ioroi, Z. Siroma, Physical Chemistry Chemical Physics 8 (6) (2006) 746.
[15] L. Kim, C.G. Chung, Y.W. Sung, J.S. Chung, Journal of Power Sources 183 (2) (2008) 524.
[16] K. Yasuda, A. Taniguchi, T. Akita, T. Ioroi, Z. Siroma, Journal of the Electrochemical Society 153 (8) (2006) A1599.
[17] E. Guilminot, A. Corcella, M. Chatenet, F. Maillard, F. Charlot, G. Berthome, C. Iojoiu, J.Y. Sanchez, E. Rossinot, E. Claude, Journal of the Electrochemical Society 154 (11) (2007) B1106.
[18] D.A. Blom, J.R. Dunlap, T.A. Nolan, L.F. Allard, Journal of the Electrochemical Society 150 (4) (2003) A414.
[19] G. Miehe, Program for Interpreting Electron Diffraction Patterns PIEP, version 7.12, Department of Materials Science, Darmstadt University of Technology, 2002.
[20] C.H. Hamann, W. Vielstich, Elektrochemie, 4. Auflage, Wiley-VCH, 2005, 650 Seiten.
[21] H.A. Gasteiger, S.S. Kocha, B. Sompalli, F.T. Wagner, Applied Catalysis B-Environmental 56 (1–2) (2005) 9.
[22] A. Ohma, S. Yamamoto, K. Shinohara, Journal of Power Sources 182 (1) (2008) 39.